3.1. Introduction

Dielectric materials have become increasingly important in the development of electronic devices due to their high values of dielectric permittivity, which allow for the fabrication of small-sized capacitors for microelectronic applications and high energy density storage [**1**, **2**]. In recent years, $CaCu_3Ti_4O_{12}$ (CCTO) with a perovskite-like structure has garnered significant interest owing to its extraordinarily high dielectric constant ($\varepsilon' \sim 10^4$) observed across an extensive range of frequencies and temperatures [**3**, **4**]. However, the large low-frequency dielectric loss (tan δ) than the suitable standard condition for capacitors prevents it from being used in practical applications. It is generally acknowledged that CCTO polycrystalline ceramics, which contain insulating grain boundaries (GBs) and n-type semiconducting grains, are electrically heterogeneous [**5**–**7**]. It has been extensively hypothesized that the internal barrier layer capacitor (IBLC) mechanism is the primary cause of the large dielectric response in CCTO ceramics [**8**, **9**]. Additionally, CCTO also displays non-ohmic characteristics, making them possible varistor components [**10**]. In CCTO polycrystalline ceramics, the electric field strength (E) and current density (J) follow a nonlinear relationship [**11**]. The Schottky barrier that is present at the grain boundaries (GBs) is believed to be the source of nonlinear J-E behaviour, while the massive ε' is widely responsible due to the electric response of GBs [**12**, **13**]. Other than that, introducing doping material into the stoichiometric ratio of CCTO has been demonstrated as a viable approach to enhance the dielectric properties of CCTO. Zheng et al. [**55**] investigated the impact of Cr dopant on CCTO properties. Through the addition of 3 mol% of Cr_2O_3, they observed an increase in the dielectric constant across the entire frequency range, spanning from 100 Hz to 1 MHz. The same sample also exhibited the highest dielectric loss. This trend may be attributed to increasing grain size with rising Cr

content. The bigger grain size may contribute to the higher dielectric constant. Other researchers [**56**] also explored the impact of grain size on the dielectric constant of CCTO ceramics. They argued that bigger grain formation can contribute to a higher dielectric constant value. Specifically, at a frequency of 10 kHz, ceramics with larger grain sizes exhibited a dielectric constant of approximately 9000, whereas samples with smaller grain sizes only demonstrated a value of around 3000. $Bi_{2/3}Cu_3Ti_4O_{12}$ (BCTO), a CCTO-like molecule that shares an isostructural relationship with CCTO, has been reported in the literature [**14**, **15**]. Even though several studies have attempted to synthesize BCTO [**16**, **17**], it is still difficult to get a large dielectric constant while retaining a relatively low dielectric loss [**18**]. Yang et al. produced BCTO using the solid-state reaction technique, yielding a high dielectric constant of about 3.3×10^5 at 1 kHz [**19**]. The synthesized BCTO samples by Gautam et al. via semi-wet method and electro ceramic synthesis, reveal a dielectric constant value of 2.9×10^4 and a dielectric loss over [**20**]. However, these figures for the dielectric losses are too high for actual practical applications. There are several methods, such as shrinking the grain size to increase the density of the grain boundary (GB) layers, adding oxygen at the GBs, and doping in BCTO with appropriate ions to raise the resistivity of the GBs, that can be used to reduce the tan δ of the BCTO ceramic by raising the resistivity at the GBs (Rgb) or enhancing the inherent electrical characteristics of the GB layers [**5**, **8**, **12**, **21**]. According to previous work reported by Rai et al. [**22**], incorporation of Ni^{2+} into BCTO ceramic can improve ε′ about 2.5×10^3. Simultaneously, tan δ was reduced to~0.08. Mohammed et al. [**57**] synthesized the Ni^{2+}-Co^{2+}-substituted BCTO and found a dielectric constant (3800) at room temperature and a frequency of 42 Hz with a relatively low loss of~0.5.

Therefore, In the present work, we have described the synthesis as well as the effect of Nd^{3+} ion substitution on the structural, dielectric, impedance, and electrical properties of $Bi_{(2/3)-x}Nd_xCu_3Ti_4O_{12}$ BNCTO ceramics with composition (x=0.05, 0.10 and 0.20) prepared using a semi-wet route.

3.2. Experimental

In this work, $Bi_{(2/3)-x}Nd_xCu_3Ti_4O_{12}$ BNCTO (x = 0.05 0.10, 0.20) ceramic was prepared by using a semi-wet route. The above ceramic composites are referred to as BNCTO-0.05, BNCTO-0.1, and BNCTO-0.2, respectively. The stoichiometric amounts of highly pure bismuth nitrate ($Bi(NO_3)_35H_2O$, 99 %), copper acetate $Cu(CH_3COO)_2$. H_2O (99% purity) titanium oxide TiO_2 (98.5% purity), Nd_2O_3 (99.99% purity) and citric acid were used as starting material and mixed in double distilled water. Details of the preparation method have been published in a previous study [**23**]. The acquired material underwent grinding and was subjected to calcination at a temperature of 1073 K for 6 h. The resulting calcined powder was then mixed with 2% polyvinyl alcohol (PVA) and compacted into disk-shaped pellets measuring 10 mm in diameter and approximately 1 mm in thickness, using a uniaxial pressure of 4–5 tons after thorough grinding. These disk-shaped pellets were subsequently sintered in an air environment at 1173 K for 8 h.

X-ray diffraction (XRD, Rigaku miniflex 600, Japan) was used to characterise the crystalline structure of sintered pellets using a CuKα source, over 2θ scanning from 20° to 80°. Meanwhile, scanning electron microscopy (SEM, ZEISS; model EVO18 research, Germany) and energy-dispersive X-ray spectroscopy (EDX, Oxford instrument, USA) were used to examine the surface microstructure and elemental composition of the samples. X-ray photoemission spectroscopy (XPS) was used to analyze the valence state of elements present

in the ceramics. A high-performance frequency LCR meter (E4980A/AL, Keysight,) was used to evaluate the dielectric characteristics and complex impedance with applied voltages in the frequency and temperature ranges of 20 Hz to 2 MHz and 303 K to 503 K, respectively.

3.3. Results and discussion

3.3.1. Microstructural studies

The crystalline structures and phase purity of BNCTO ceramic with different compositions (x=0.05, 0.10, and 0.20) were investigated using XRD techniques as shown in Figure **3.1**. It can be seen from Figure **3.1** (a) that the main diffraction peaks in the XRD profiles for all samples could be perfectly indexed by a body-cantered cubic perovskite-like structure of space group Im-3 which shows the presence of BCTO, which can be justified (JCPDS card no.75–2188). Furthermore, Nd^{3+} doping ions led to the development of a weak refection peak at 27.43^{o}, corresponding to the (110) crystalline plane of rutile TiO_2 as the second phase in BNCTO-0.2 [**24**]. Some of the impurity phase may be due to TiO_2 being visible in the XRD pattern of the BNCTO samples between 25 and 28 in the case of the higher concentration of Nd-doped BCTO. Since these impurity phases do not occupy their lattice position in the crystal, so, therefore, they appear in the XRD as impurities. The enlargement view of the most instance peaks in the XRD spectrum is shown in Figure **3.1** (b), clearly revealing that the peak was shifted towards a higher angle that has witnessed the successful incorporation of Nd in BCTO ceramic. The average crystallite size calculated using the Debye-Scherrer equation [**25**–**27**] was determined to decrease with the rise of Nd concentration in BCTO ceramics and is shown in Table **1**

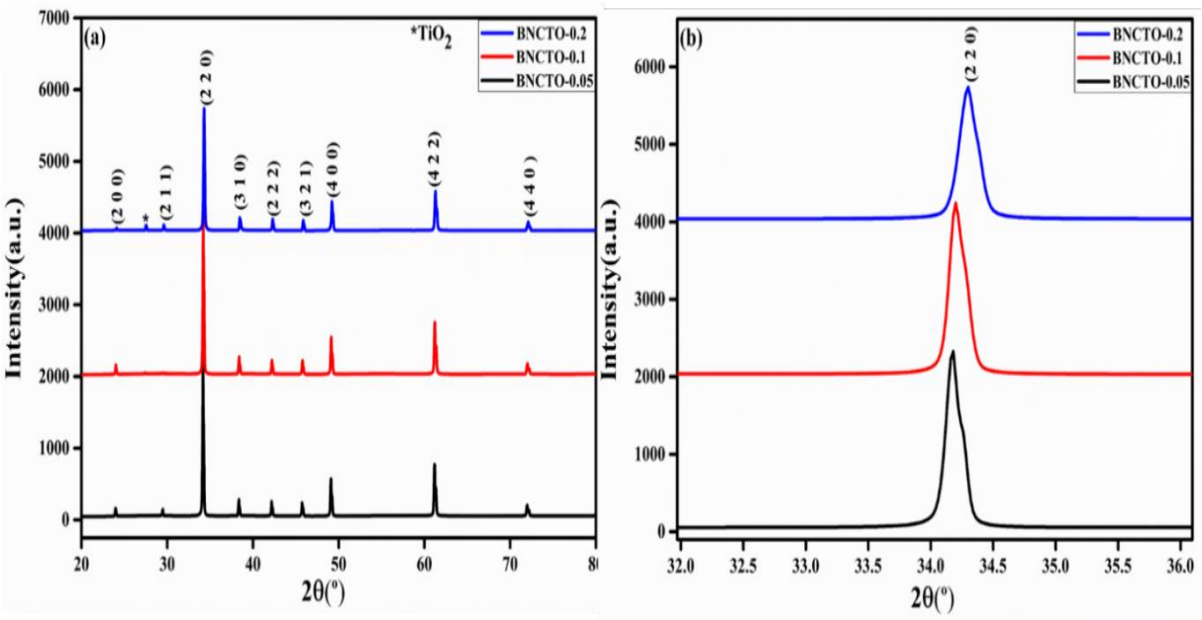

Fig. 3.1 (a) X-ray diffraction (XRD) pattern and (b) Magnified XRD pattern in the enlarged region ($32° < 2\theta < 36°$) of $Bi_{(2/3)-x}Nd_xCu_3Ti_4O_{12}$ BNCTO (x = 0.05 0.10, 0.20) ceramics.

The Rietveld refinement was done by using FULLPROF software to further elucidate the structure of BNCTO ceramic with a few selected compositions such as x=0.05, 0.10, and 0.20, respectively, as shown in Figure **3.2**. The Rietveld refinement fitting of the XRD pattern shows the presence of a cubic structure of the BNCTO ceramic with a space group of Im-3. The parameters identified during Rietveld refinement such as the expected R-factor (R_{exp}), profile R-factor (R_p), and weighted profile R-factor (R_{wp}), for all selected compositions, were presented in Table **1**. Furthermore, the goodness-of-fit (GOF) factors were identified to be between 1.47 and 1.39. These suitable values for the refinement parameters demonstrate the reliability of the refined structural parameters. The Rietveld refinement structural parameters clearly showed that Nd ions indeed entered the lattice location for Bi. The lattice parameter decreased as Nd substitution increased, primarily because the ionic radius of Nd^{3+} is smaller than that of the Bi^{3+} host ions [**28**].

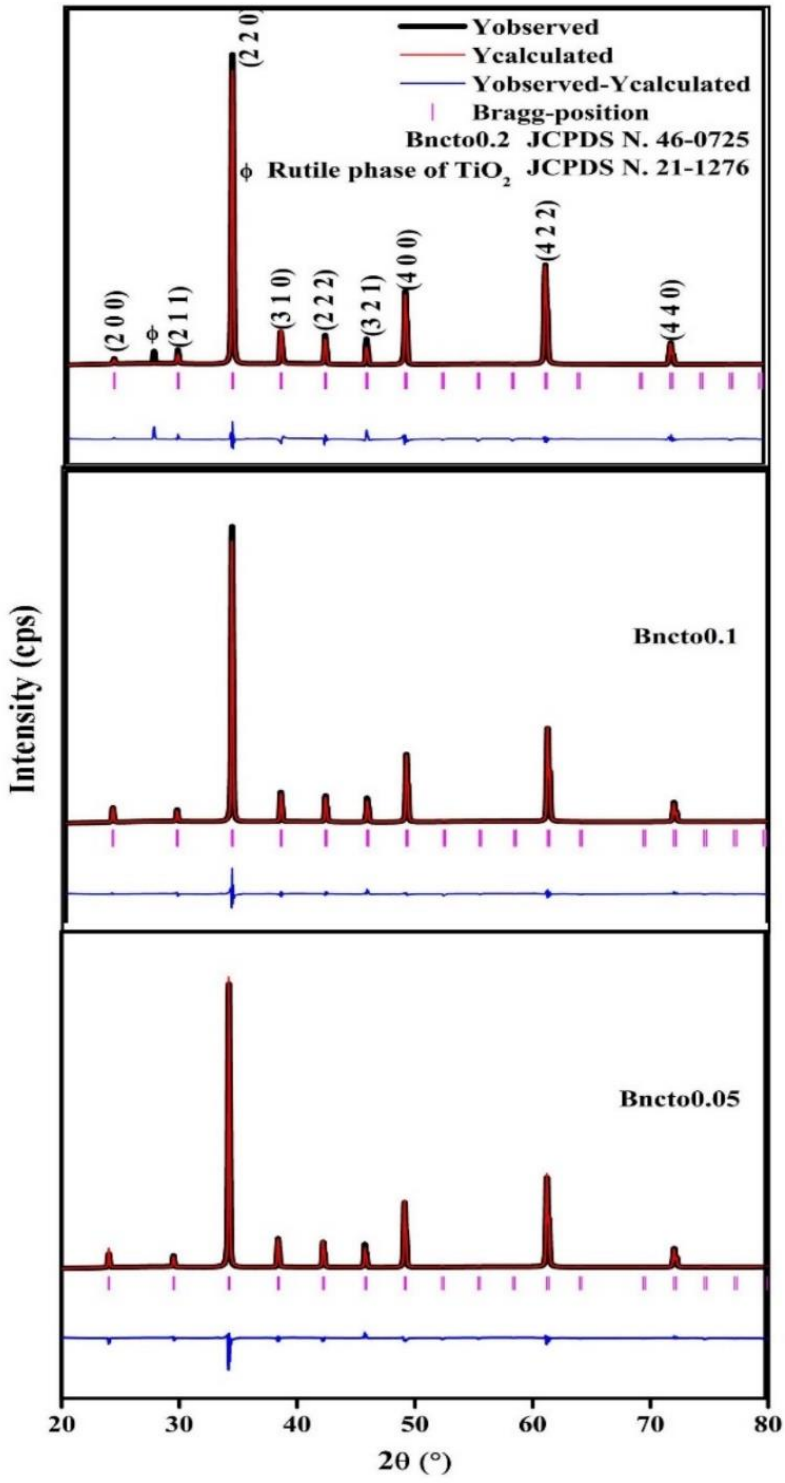

Fig. 3.2 Rietveld refinement profile of $Bi_{(2/3)-x}Nd_xCu_3Ti_4O_{12}$ (x = 0.05 0.10, 0.20) ceramics.

Table 3.1 describes conditions of refinements, the refined parameters calculated through the Rietveld refinements such as Chi-square, space group, Bragg's- R factor, RF-factor, Lattice parameters, FWHM parameters, and conventional Rietveld R-factors of BNCTO ceramic with Nd compositions 0.05,0.1 and 0.2, respectively.

Conditions for refinement, wavelength (λ)= 1.54 Å and no of cycle used during refinement (=20) and no of steps per second =0.02 °/sec

	BNCTO-0.05	BNCTO-0.1	BNCTO-0.02
χ^2	0.157	0.106	0.130
space group	Im-3	Im-3	Im-3
Crystallite size (nm)	84.72	80.14	72.60
Lattice parameters (Å)	a = b = c= 7.412687	a = b = c=7.412659	a = b = c= 7.412654
Vcell ($Å^3$)	407.3171	407.3071	407.3063
FWHM parameters	U= 0.031323 V= -0.005832 W= 0.010102	U= 0.030963 V= -0.005562 W= 0.010047	U= 0.030895 V= -0.005562 W= 0.010066
Conventional Rietveld R-factors			
R_p(%) R_{wp}(%) R_{exp}(%) Bragg's R-factor (%) RF-factor (%)	17.1 11.6 29.34 7.723 5.235	13.7 9.53 29.32 3.728 2.538	14.8 10.6 29.32 4.890 3.981

Scanning electron microscopy (SEM) was employed to investigate the microstructure of Nd-doped BCTO ceramic with respective compositions of 0.05, 0.10, and 0.20, which clearly shows the presence of granular cubic shape of the grains. A notable impact on the microstructure of BCTO ceramic has been seen in the case of an introduction of Nd^{3+} ions as dopants as demonstrated in Figure **4.3** (a–c). It is observed from the figure that as the dopant concentration increases, abnormal grain growth became the dominant phenomenon, and when

a smaller ionic radius of Nd^{3+} ions was introduced to substitute the larger ionic radius of Bi^{3+} ions in pristine BCTO, it led to an increased suppression of grain development rates. Consequently, this resulted in a reduction in crystallite size and particle sizes, which in turn altered the morphology of the BNCTO ceramic. The average grain size for the BNCTO ceramic with few selected compositions (x=0.05, 0.10, and 0.20) was analyzed through ImageJ software and approximately 0.83 μm, 0.65 μm, and 0.641 μm, respectively. The reduction in grain size could be attributable to the suppression of oxygen vacancy, which inhibits particle growth [**29**]. EDS analysis was employed to validate the elemental composition across all samples, as depicted in Figure **3.3** (d–f) which emphasized the presence of Bi, Nd, Cu, Ti, and O elements in the Nd-doped BCTO ceramic. The inset of the EDS image provides the weight percentage (Wt%) and atomic percentage (At%) for all the selected compositions

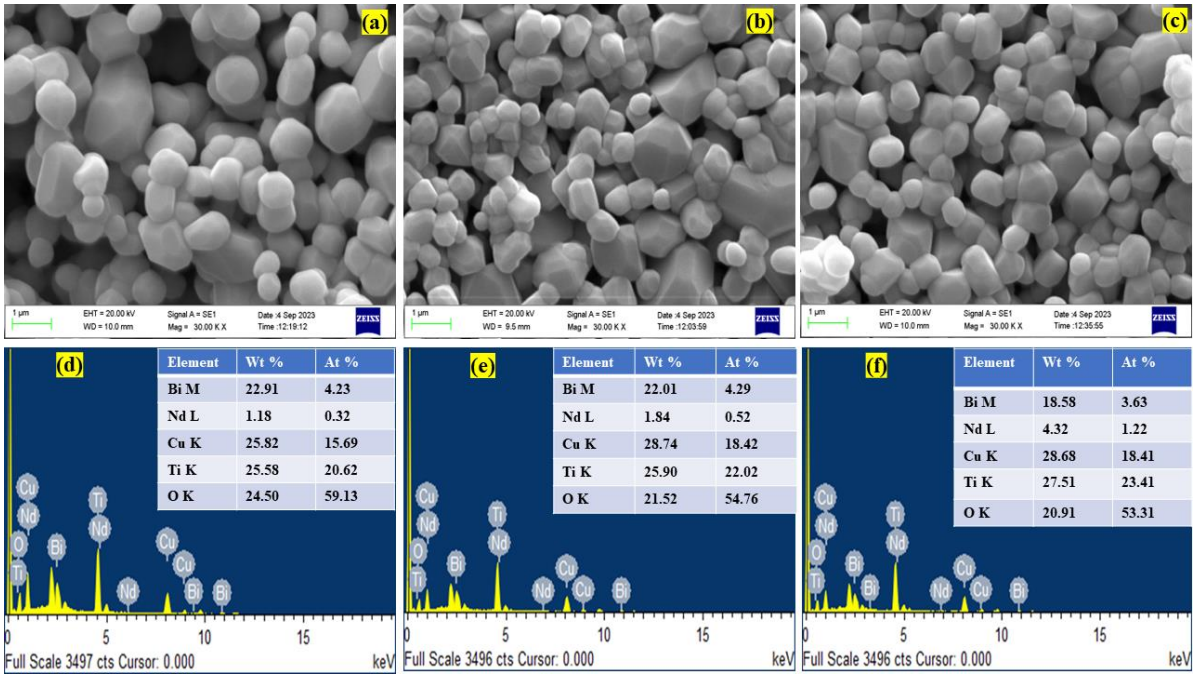

Fig. 3.3 (a–c) SEM micrographs and (d-f) EDS spectrum of $Bi_{(2/3)-x}Nd_xCu_3Ti_4O_{12}$ (x = 0.05 0.10, 0.20) ceramics.

The influence of Nd^{3+} doping on the surface morphology of BCTO ceramics was examined using AFM. This examination confirmed the presence of a granular microstructure, as depicted in Figure **3.4**. In Figure **3.4** (a-c), the 3D AFM images of the ceramics illustrate a reduction in surface root mean square roughness (R_{rms}) as the proportion of Nd^{3+} ions increase, with corresponding values of 255 nm, 158 nm, and 125 nm, respectively. Furthermore, an analysis of the grain size distribution curves from the AFM images (Figure **3.4** (d-f)) revealed a decrease in grain sizes as the Nd^{3+} doping concentration increased from x = 0.05 to x = 0.20. Both SEM and AFM observations corroborate that Nd^{3+} doping effectively suppresses grain growth.

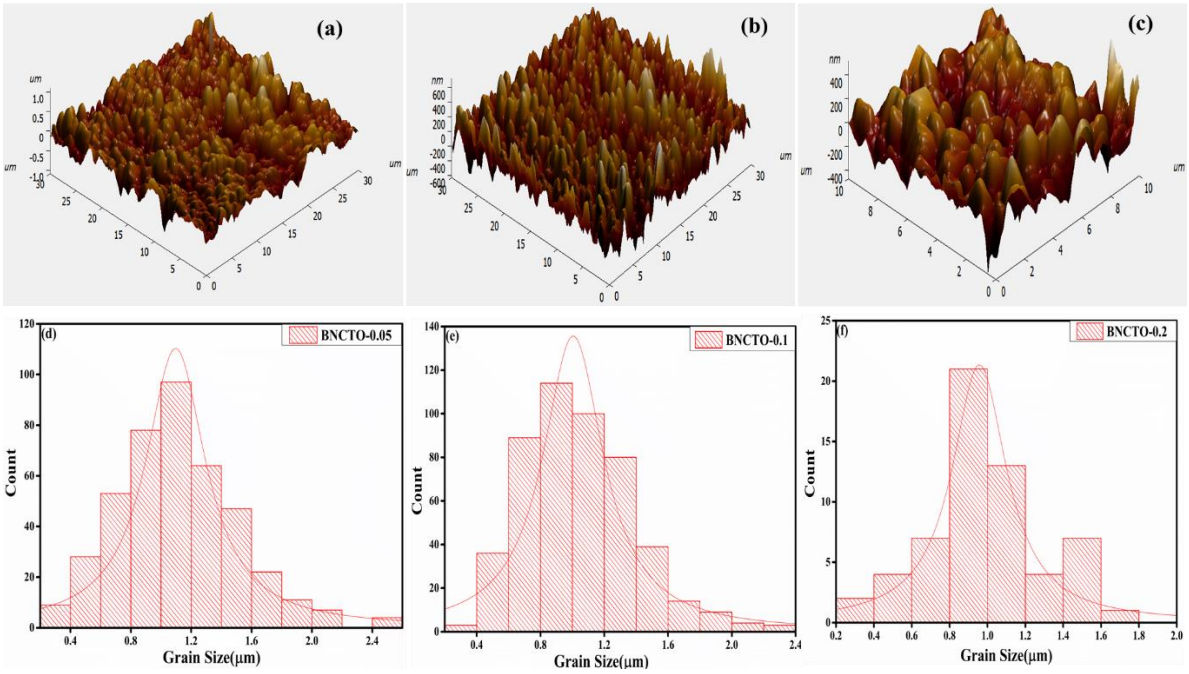

Fig. 3.4 (a-c) 3D AFM image and (d-f) the grain size distribution statistics $Bi_{(2/3)-x}Nd_xCu_3Ti_4O_{12}$ (x = 0.05 0.10, 0.20) ceramics.

X-ray photoelectron spectroscopy (XPS) analysis was conducted to elucidate the electronic structure and valence state of BNCTO-0.2 ceramic, as depicted in Figure **3.5** (a-f). Figure **3.5** (a) is the survey scan XPS spectra of BNCTO-0.2 with the calibrated binding energy of C 1s.

In Figure **3.5** (b), the high-resolution core level XPS spectrum of Bi 4f reveals two prominent peaks, situated at 158.18 and 163.49 eV, corresponding to Bi $4f_{7/2}$ and Bi $4f_{5/2}$, respectively [**30**]. The presence of these Bi peaks confirms the +3-oxidation state of bismuth in the compound. Furthermore, as demonstrated in Figure **3.5** (c), the appearance of peaks at 973.78 eV and 981.78 eV in the Nd $3d_{5/2}$ XPS spectrum of Nd-doped BCTO corresponds to Nd^{3+} ions [**31**, **32**]. These observed binding energies affirm the trivalent state of Nd ions in the material. Figure **3.5** (d) displays the XPS spectra of Cu in BCTO-0.2 ceramic, with peaks at approximately 933.27 and 953.18 eV corresponding to Cu $2p_{3/2}$ and Cu $2p_{1/2}$, respectively, confirming the presence of Cu^{2+} [**33**]. Similarly, Figure **3.5** (e) presents the XPS spectra of Ti 2p, revealing a binding energy of 459.01 eV and 456.25 eV for Ti^{3+} and reported binding energies of 457.47 and 463.43 eV for Ti^{4+} in BNCTO-0.2 ceramic [**34**]. Lastly, Figure **3.5** (f) depicts the O 1s spectra of the two samples, which display three distinct peaks located at 529.01 eV, 530.29 eV, and 532.04 eV. These peaks correspond to lattice oxygen (O_L), oxygen vacancy (V_O) defects, and oxygen associated with the -OH group or absorbed oxygen, respectively [**35**, **36**].

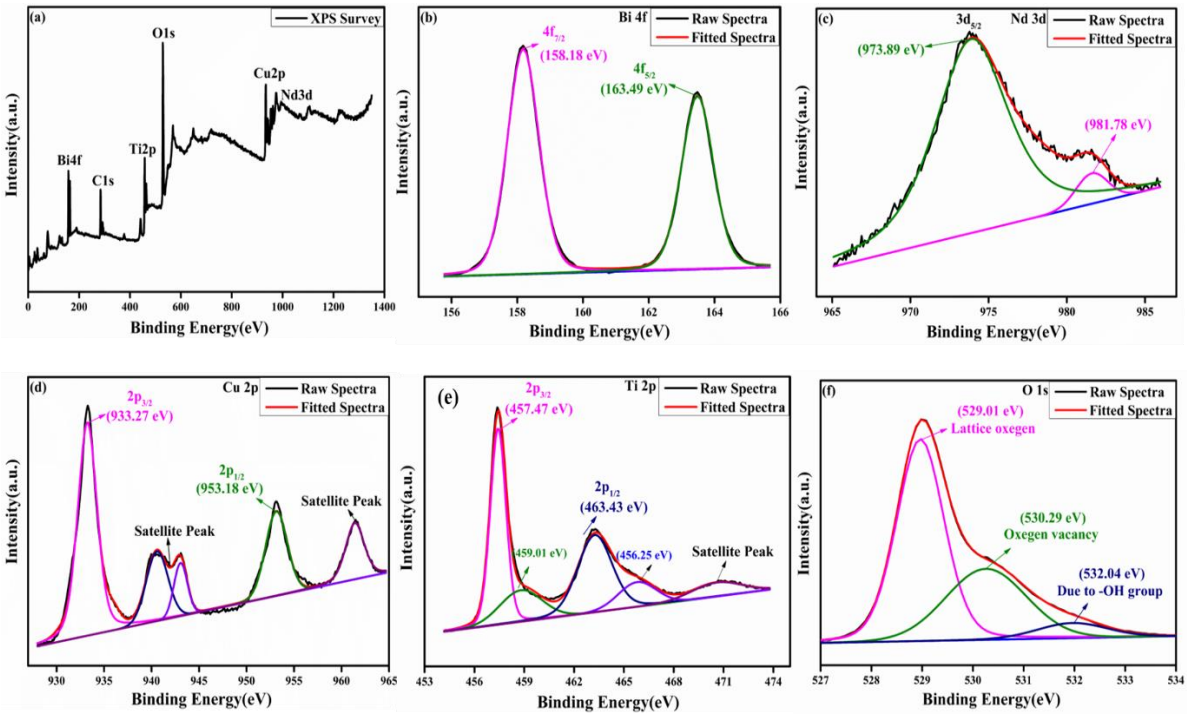

Fig. 3.5 XPS spectra of (a) XPS survey (b) Bi, (c) Nd, (d) Cu, (d) Ti, and (e) O of BNCTO-0.2 ceramic.

3.3.2. Dielectric Studies

Figure **3.6** (a, b) demonstrates the temperature variation with a dielectric constant (ε′) and tangent loss (tan δ) of BNCTO for measured compositions (x=0.05–0.20 at a fixed frequency (1 kHz)). The dielectric constant is virtually independent from 303 to 400 K and then increases dramatically with temperature, as seen in Figure **3.6** (a). The value of ε′ for BNCTO samples is less than that reported for undoped BCTO [**20**], as seen in Figure **3.6** (a). At 303 K, the dielectric constants of Nd-doped BCTO with x=0.50, 0.10, and 0.20 are approximately 175, 386, and 45, respectively. Figure **3.6** (b) depicts the temperature-dependent variation of tan δ values at 1 kHz for various compositions of doped BCTO ceramics. The figure illustrates that tan δ becomes temperature-independent at lower temperatures but exhibits a significant rise as the temperature increases. In contrast, tan δ remained low until 400 K (Figure **3.6** (b))

and then increased over time, indicating that dc conductivity increased at high temperatures [**50**].

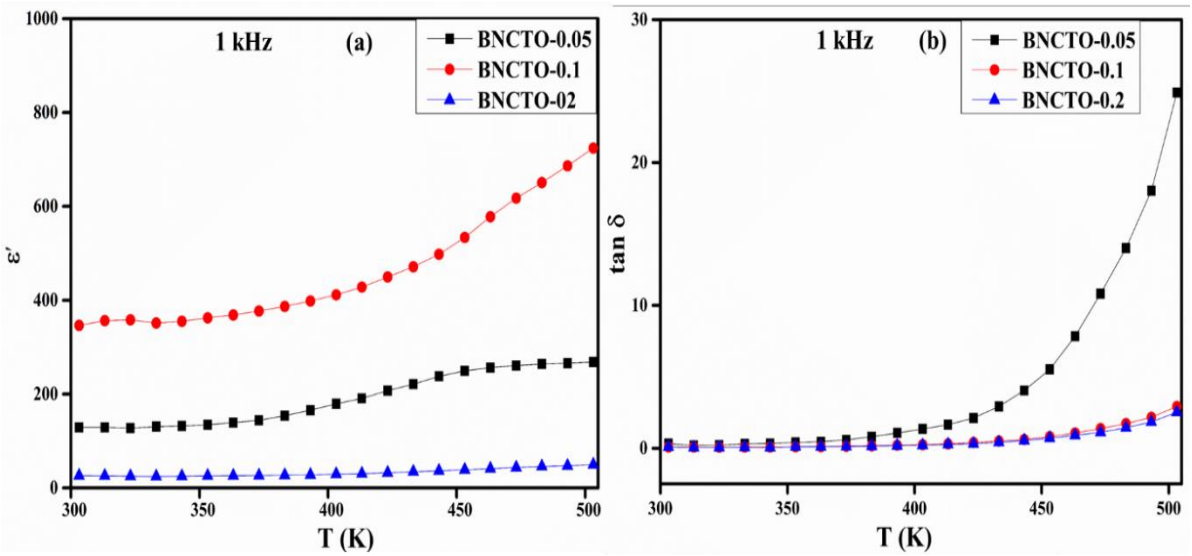

Fig. 3.6 (a) Temperature dependence of ε′ and (b) tan δ at 1 kHz of $Bi_{(2/3)-x}Nd_xCu_3Ti_4O_{12}$ (x = 0.05 0.10, 0.20) ceramics.

Figure **3.7** (a) demonstrates variation in the dielectric permittivity (ε′) of different Nd-doped BCTO ceramic sintered at 1173 K for 8 h as a function of frequency and at 303 K. It is clear that doping with Nd ions had a significant influence on the BCTO ceramic. The ε′ in the lower frequency region decreases with a rise in frequency but is almost independent in the frequency range 10^3 –10^7 Hz. A significant decrease in the ε′ values of the Nd-doped BCTO was found to be mainly consistent with their microstructures, which corresponds to the IBLC model. The dielectric permittivity of the system can be roughly calculated using the relationship below, assuming that the grains are adequately conducting [**37**, **38**].

$$\varepsilon' = \varepsilon_{gb} \frac{A}{t} \qquad 3.1$$

where ε_{gb}, A, and t represent the grain boundary permittivity, grain average size, and grain boundary average thickness, respectively. The above equation evident that the dielectric constant of BCTO ceramics diminishes with a reduction in grain size. Moreover, the densification of BCTO samples can also contribute to the dielectric constant, whereas the existence of pores in BCTO can reduce the dielectric constant in these samples [**47**, **48**]. The ε' values at 1 kHz and 303 K were found to be ~$3.90\times 10^{2,}$ 5.20×10^{2}, and 75 for BNCTO-0.05, BNCTO-0.1, and BNCTO-0.2, respectively. Figure **3.7** (b) illustrates the dielectric loss (tan δ) values of the Nd-doped BCTO ceramic at 303 K as a function of frequency. According to the figure, the low-frequency tan δ values of the BNCTO ceramics were significantly lower than those of the undoped BCTO ceramic [**20**]. The illustration also demonstrates that the dielectric loss in doped BCTO samples decreases as the frequency increases up to 1 kHz. Beyond this point, it remains nearly constant for all three compositions until 600 kHz. At higher frequencies, specifically above 1 MHz, all compositions exhibit a pronounced upward trend in dielectric loss, which has been previously observed and documented by other researchers [**49**]. The change in ε' was strongly connected to the variation of tan δ caused by the dopant ions. The tan δ values of BNCTO ceramic with selected compositions (x=0.05, 0.10, and 0.20) were obtained to be 0.315, 0.090, and 0.056, respectively, at 1 kHz. The rise in grain boundary resistance (R_{gb}) which is correlated with the density of the insulating layer in the grain boundaries may be the cause of the low values of tan δ in ceramic [**39**].

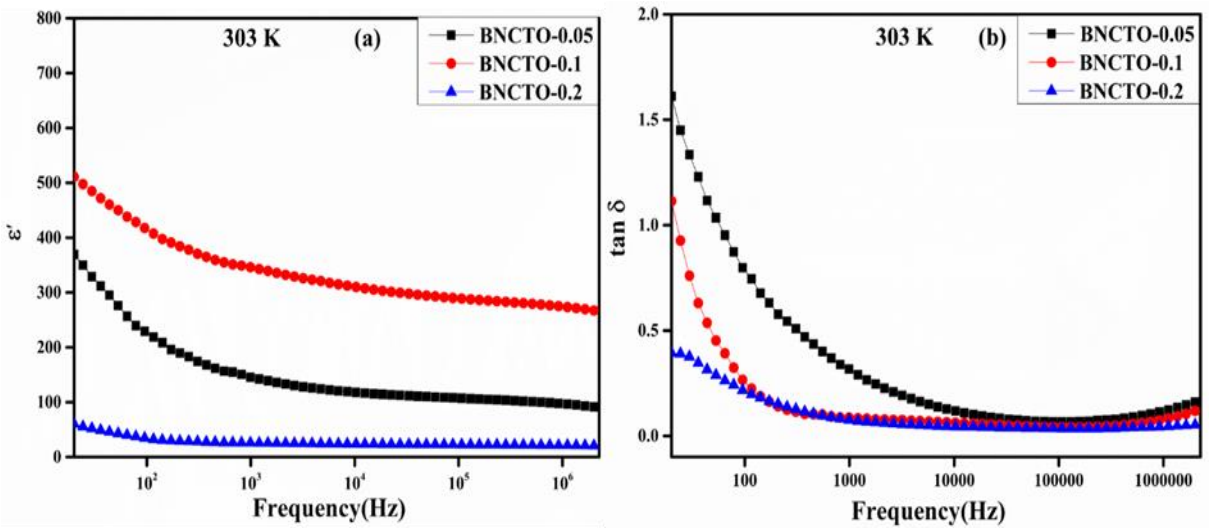

Fig. 3.7 (a) Variation of dielectric constant and (b) tangent loss with frequencies for all three concentrations of BNCTO ceramics at 303 K.

To determine the cause of the decrease in the dielectric loss for $Bi_{(2/3)-x}Nd_xCu_3Ti_4O_{12}$ (x=0.05, 0.10, and 0.20), the complex impedance analysis (Z″ against Z′) was performed at various temperatures, and 303 K is shown in Figure **3.8**. According to Figure **3.8** (a–c), two semicircular arcs with different intercepts were found for a few temperatures of BNCTO ceramic, which may be attributed to the contribution of grain boundary effect and electrode surface effects, and the rest single semicircular arcs at different temperatures of the samples, which may be due to contribution of grain boundary effect only. Semicircular arcs are on the low-, middle-, and high-frequency sides due to electrode, grain boundary, and grain contributions, respectively. The grain boundary behaviour of the sample was impacted by the parallel interplay of grain boundary resistance (R_{gb}) and grain boundary capacitance (C_{gb}). This interplay supports the presence of the internal barrier layer capacitance mechanism, which is a distinctive characteristic of materials featuring semiconducting grains and insulating grain boundaries. The electrode resistance arises at a few observed temperatures, which could be attributed to electrode polarization effects in BNCTO ceramics. The diagram

vividly demonstrates that with increasing temperature, the diameter of semicircles decreases, leading to a reduction in overall resistivity. This phenomenon signifies the emergence of a thermally induced conduction mechanism within the grains and at their boundaries [**51**, **52**]. This electrical behaviour underscores the significant influence of temperature on the electrical characteristics of both grains and grain boundaries. Figure **3.8** (d) depicts the complex impedance plot of BNCTO ceramics with different compositions at 303 K. As depicted in the figure, it is evident that partial or incomplete semicircular arcs were detected in all BNCTO ceramics. These observations can be attributed to the presence of grain boundary resistance and electrode resistance (in the case of BNCTO-0.2). Additionally, a detailed examination of the high-frequency region reveals minimal alteration in grain resistivity (R_g) with the introduction of Nd doping, as illustrated in the inset of Figure **3.8** (d). The values of R_g (calculated from nonzero intercept) for the BNCTO ceramics with varied concentrations (x=0.05, 0.10, and 0.20) at higher frequencies were around 50 Ω, 72 Ω, and 110 Ω, respectively. It is also noted that when the concentration of Nd increases, the size of the arc (i.e., resistance) diminishes. The R_{gb} of the BNCTO ceramic at various compositions was computed from the arc and found to be 2.21×10^7 Ω, 2.34×10^7 Ω, and 7.77×10^7 Ω for BNCTO-0.05, BNCTO-0.1, and BNCTO-0.2, respectively. The reduction in tan δ values can be ascribed to the rise in R_{gb} values, and this connection states that R_{gb} should be inversely proportional to low frequency tan δ [**8**, **40**]. A variation in the relatively large R_{gb} value, which is exacerbated by the substitution of Nd^{3+} ions, is connected with a variance in the decreasing tan δ value [**41**].

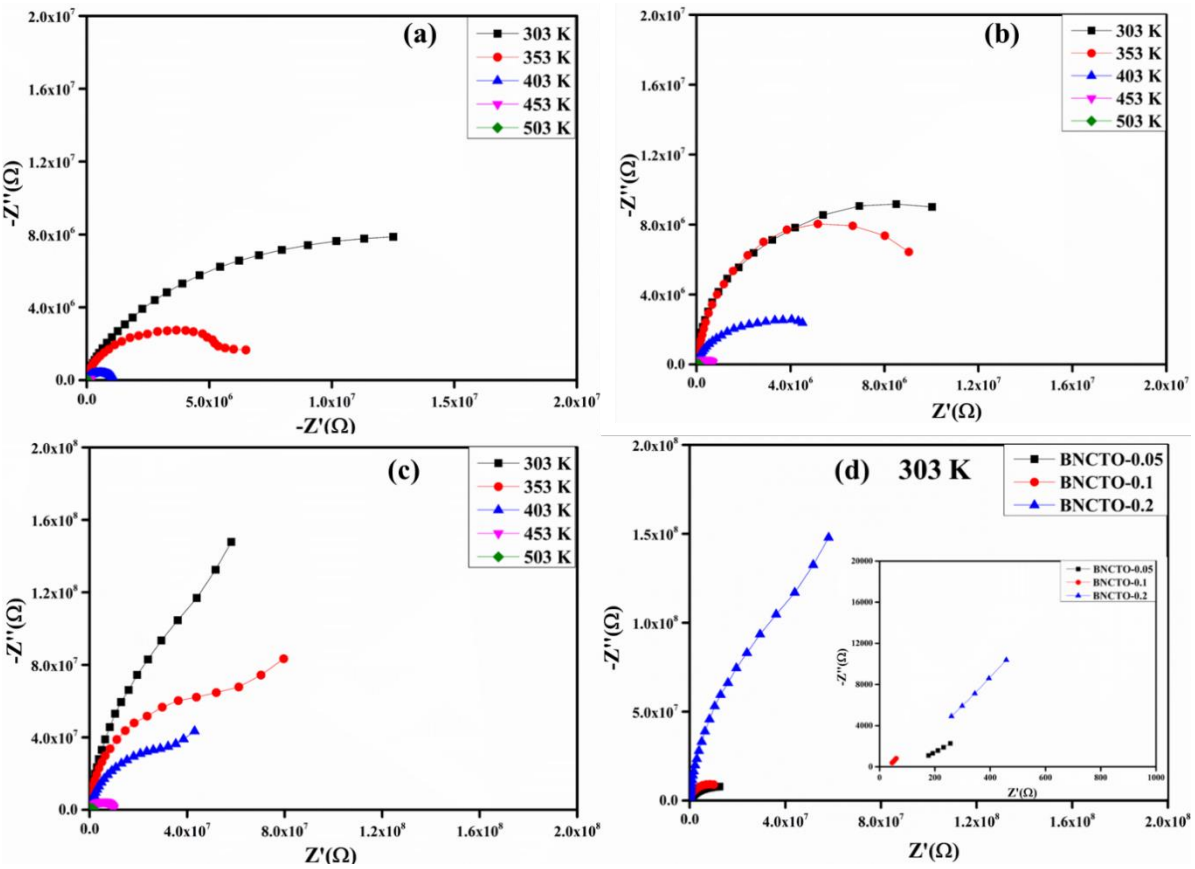

Fig. 3.8 (a–c) Variation of Z′ with Z″ at different temperatures and (d) at 303 K of three different concentrations of Nd (x =0.05,0.10, and 0.20) doped BCTO.

Figure **3.9** illustrates the variation of Z″ with frequency across different temperatures and at 303 K, for $Bi_{(2/3)-x}Nd_xCu_3Ti_4O_{12}$ ceramic with x values of 0.05, 0.10, and 0.20. As depicted in Figure **3.9** (a–c), the positions of the relaxation peaks shift towards higher frequencies as the temperature rises. Additionally, the widening of the relaxation peaks and the decrease in the maximum Z″ value as temperature increases indicate the presence of a temperature-dependent relaxation phenomenon in these ceramics. The relaxation process occurs owing to defects and vacancies at higher temperatures [**53**, **54**]. In Figure **3.9** (d), it is also observed that with the increase of concentration, peaks of Z″ shift towards the high-frequency region. This demonstrates that concentration-dependent relaxation behaviour also exists in a ceramic [**42**].

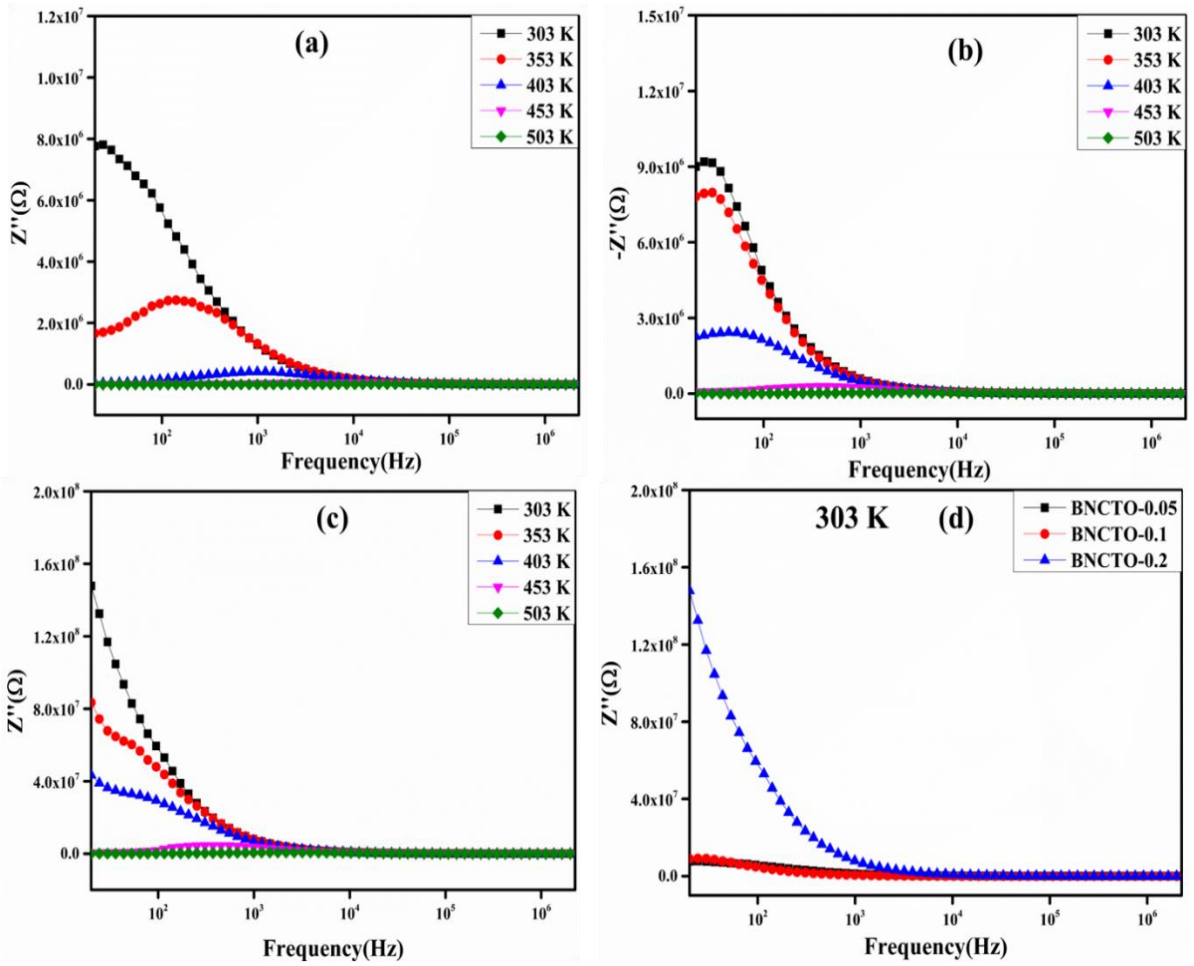

Fig. 3.9 (a-c) Variation of Z″ with frequency at different temperatures and (d) at 303 K of $Bi_{(2/3)-x}Nd_xCu_3Ti_4O_{12}$ (x = 0.05 0.10, 0.20) ceramics.

Furthermore, the behavior of the temperature-dependent estimated σ_{ac} and activation energy of the $Bi_{(2/3)-x}Nd_xCu_3Ti_4O_{12}$ (x = 0.05, 0.10, and 0.20) ceramics were estimated using the Arrhenius equation given as [**43**]:

$$\sigma(T) = \sigma_0 exp\left(\frac{-E_a}{k_b T}\right) \qquad 3.2$$

where σ(T) represents the electrical conductivity, Ea stands for the activation energy, T denotes the temperature in Kelvin, k_b is the Boltzmann constant, and σ_0 signifies the pre-exponential term. Figure **10** (a) depicts the variance of the log σ vs. 1000/T curve at 1 kHz in

the temperature range 303-503 K. In all compounds, the conductivity of the materials increases as the temperature rises. The activation energies (E_a) were computed and found to be 0.75 eV, 0.80 eV, and 0.86 eV for various concentrations of BNCTO ceramics respectively. The activation energy of the materials was gradually boosted. The substitution of a minor amount of Nd in BCTO is responsible for the slight increase in the electrical conductivity of the material. Typically, a rise in E_a value indicates a decrease in oxygen vacancies, implying that fewer electrons can flow through the potential barrier, reducing σ and benefiting the decrease of tan δ.

Figure **10** (b) represents the frequency-dependent ac electrical conductivity (σ_{ac}) at 303 K for various samples of $Bi_{(2/3)-x}Nd_xCu_3Ti_4O_{12}$ (where x = 0.05, 0.10, and 0.20). The frequency-dependent conductivity is typically consistent with Jonscher's power law and is determined using the following equation [**44**].

$$\sigma_{ac} = \sigma_{dc} + A\omega^s \qquad 3.3$$

where A and exponent s are temperature- and material-dependent constants, and ω is the angular frequency. The word $A\omega^s$ describes all dispersion phenomena and gives information about the ac dependency. The exponent "s" typically falling within the range of $0 < s < 1$, serves as a means to ascertain the extent of interaction between the mobile ion and the lattice that surrounds it [**45**]. This law states that the cause of the variation in conductivity with frequency is related to the motion of mobile charge carriers during the relaxation process [**44**]. The values of s for all BNCTO ceramics are found to be 0.86, 0.89, and 0.68 respectively. The values of s decline with a rise in concentration which indicates the decrease in conductivity. Moreover, the electrical conductivity of BNCTO ceramics exhibited a consistent

rise as the frequency exceeded 1 kHz which is attributed to the hopping conduction characteristic of the ceramics [**46**].

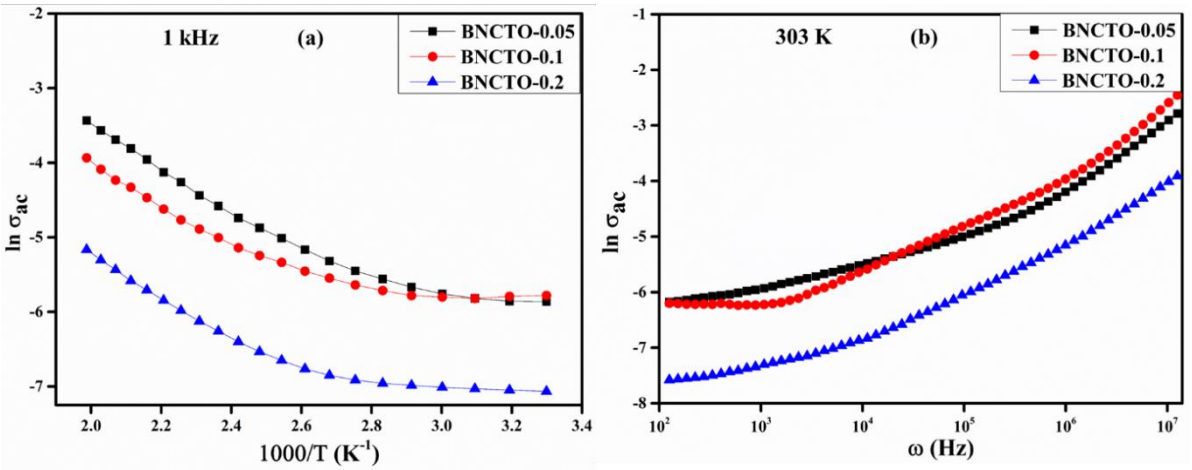

Fig. 3.10 (a) Temperature-dependent ac conductivity and (b) Frequency-dependent ac conductivity of BNCTO ceramics.

3.4. Conclusions

In conclusion, the dielectric behaviour of $Bi_{(2/3)-x}Nd_xCu_3Ti_4O_{12}$ ceramic with compositions x=0.05, 0.10, and 0.20, was studied using a semi-wet route approach. The Rietveld refinement using the FULLPROF program verifies the cubic phase formation for all selected compositions of BNCTO ceramic with space group of Im-3, and decreases in crystallite size were also observed in the case of increase in concentrations of Nd^{3+} ions in the BCTO ceramic. The microstructure and elemental compositions of Nd-doped BCTO ceramic were investigated through SEM and EDX analysis, confirming granular-shaped grains and the presence of Bi, Nd, Cu, Ti, and O elements, respectively, in the synthesized materials. The grain size obtained from the SEM analysis was observed in decreasing order with a rise in concentrations of Nd^{3+} ions which was also verified by the AFM analysis. The electronic state of the BNCTO ceramic was confirmed by the XPS investigation. The investigation of

dielectric characteristics reveals that the dielectric loss at higher frequencies is less than one, emphasizing that the synthesized material can be a good option of material for high-frequency applications. Complex impedance spectroscopy tests validated the grain and grain boundary effect. The activation energy value was found to be increasing manner on successive substitutions of Nd^{3+} ions in BCTO ceramic and observed in the range of 0.75–0.86v eV, suggesting to electrical conduction in BNCTO ceramic due to mobility of the ionized oxygen defects.

3.5. References

[1] B. Peng, Q. Zhang, Y. Lyu, L. Liu, X. Lou, C. Shaw, H. Huang, Z. Wang, "Thermal strain induced large electrocaloric effect of relaxor thin film on $LaNiO_3$/Pt composite electrode with the coexistence of nanoscale antiferroelectric and ferroelectric phases in a broad temperature range," Nano Energy, **47** (2018) 285-293.

[2] B. Peng, Q. I. Zhang, B. Gang, G. I. Leighton, C. Shaw, S. J. Milne, B. Zou, W. Sun, H. Huang, Z. Wang, "Phase-transition induced giant negative electrocaloric effect in a lead-free relaxor ferroelectric thin film," Energy & Environmental Science, **12** (2019) 1708-1717.

[3] Z. Peng, P. Liang, X. Wang, H. Peng, Y. Xiang, X. Chao, Z. Yang, "Copper cadmium titanate prepared by different methods: phase formation, dielectric properties and relaxor behaviors," Ceramics International, **44** (2018) 7814-7823.

[4] R. Espinoza-González, S. Hevia, Á. Adrian, "Effects of strontium/lanthanum co-doping on the dielectric properties of $CaCu_3Ti_4O_{12}$ prepared by reactive sintering," Ceramics International, **44** (2018) 15588-15595.

[5] S. De Almeida-Didry, M. N. Nomel, C. Autret, C. Honstettre, A. Lucas, F. Pacreau, F. Gervais, "Control of grain boundary in alumina doped CCTO showing colossal permittivity by core-shell approach," Journal of the European Ceramic Society, **38** (2018) 3182-3187.

[6] L. Ren, L. Yang, C. Xu, X. Zhao, R. Liao, "Improvement of breakdown field and dielectric properties of $CaCu_3Ti_4O_{12}$ ceramics by Bi and Al co-doping," Journal of Alloys and Compounds, **768** (2018) 652-658.

[7] X. Huang, H. Zhang, Y. Lai, J. Li, "The lowered dielectric loss tangent and grain boundary effects in fluorine-doped calcium copper titanate ceramics," Applied Physics A, **123** (2017) 1-7.

[8] W. Li, L. Tang, F. Xue, Z. Xin, Z. Luo, G. Du, "Large reduction of dielectric losses of $CaCu_3Ti_4O_{12}$ ceramics via air quenching," Ceramics International, **43** (2017) 6618-6621.

[9] J. Boonlakhorn, N. Chanlek, J. Manyam, P. Srepusharawoot, S. Krongsuk, P. Thongbai, "Enhanced giant dielectric properties and improved nonlinear electrical response in acceptor-(Al^{3+}, Ta^{5+})-substituted $CaCu_3Ti_4O_{12}$ ceramics," Journal of Advanced Ceramics, **10** (2021) 1243-1255.

[10] E. Swatsitang, S. Nijpanich, S. Putjuso, T. Putjuso, "Effect of sintering temperature and Sm^{3+} doping on the dielectric properties and non-Ohmic behavior of $Ca_{1-1.5x}Sm_xCu_3Ti_{4-2}O_{12}$ (x= 0.05 and 0.10) ceramics," Results in Physics, **30** (2021) 104896.

[11] J. Jumpatam, B. Putasaeng, N. Chanlek, J. Manyam, P. Srepusharawoot, S. Krongsuk, P. Thongbai, "Influence of Sn and F dopants on giant dielectric response and Schottky potential barrier at grain boundaries of CCTO ceramics," Ceramics International **47** (2021) 27908-27915.

[12] J. Jumpatam, B. Putasaeng, N. Chanlek, P. Kidkhunthod, P. Thongbai, S. Maensiri, P. Chindaprasirt, "Improved giant dielectric properties of $CaCu_3Ti_4O_{12}$via simultaneously tuning the electrical properties of grains and grain boundaries by F^- substitution," RSC Advances, **7** (2017) 4092-4101.

[13] P. Saengvong, J. Boonlakhorn, N. Chanlek, B. Putasaeng, P. Thongbai, " Giant dielectric permittivity with low loss tangent and excellent non− Ohmic properties of

the (Na^{+}, Sr^{2+}, Y^{3+}) $CaCu_3Ti_4O_{12}$ ceramic system," Ceramics International, **46** (2020) 9780-9785.

[14] Z. Yang, P. Liang, L. Yang, P. Shi, X. Chao, Z. Yang, "Synthesis, dielectric properties of $Bi_{2/3}Cu_3Ti_4O_{12}$ ceramics by the sol–gel method," Journal of Materials Science: Materials in Electronics, **26** (2015) 1959-1968.

[15] L. Yang, X. Chao, P. Liang, L. Wei, Z. Yang, "Electrical properties and high-temperature dielectric relaxation behaviors of $NaxBi_{(2-x)/3}Cu_3Ti_4O_{12}$ ceramics," Materials Research Bulletin, **64** (2015) 216-222.

[16] Z. Yang, P. Liang, L. Yang, P. Shi, X. Chao, Z. Yang, "Synthesis, dielectric properties of $Bi_{2/3}Cu_3Ti_4O_{12}$ ceramics by the sol–gel method, " Journal of Materials Science: Materials in Electronics, **26** (2015) 959–1968.

[17] L. Yang, X. Chao, Z. Yang, N. Zhao, L. Wei, Z. Yang, "Dielectric constant versus voltage and non-Ohmic characteristics of $Bi_{2/3}Cu_3Ti_4O_{12}$ ceramics prepared by different methods, " Ceramics International, **42** (2016) 2526–2533.

[18] P. Liang, Y. Li, F. Li, X. Chao, Z. Yang, "Effect of the synthesis route on the phase formation behavior and electric property of $Na_{0.5}Bi_{0.5}Cu_3Ti_4O_{12}$ ceramics," Materials Research Bulletin, **52** (2014) 42-49.

[19] L. Yang, G. Huang, T. Wang, H. Hao, Y. Tian, "Colossal dielectric permittivity and relevant mechanism of $Bi_{2/3}Cu_3Ti_4O_{12}$ ceramics," Ceramics International, **42** (2016) 9935–9939.

[20] P. Gautam, A. Khare, S. Sharma, N. B. Singh, K. D. Mandal, "Characterization of $Bi_{2/3}Cu_3Ti_4O_{12}$ ceramics synthesized by semi-wet route," Progress in Natural Science: Materials International, **26** (2016) 567-571.

[21] J. Guo, L. Sun, Q. Ni, E. Cao, W. Hao, Y. Zhang, Y. Tian, L. Ju. " Dielectric properties and nonlinear I-V electrical behavior of ($Ni^{2+,}$ $Zr^{4+)}$ co-doping $CaCu_3Ti_4O_{12}$ ceramics," Applied Physics A, **124** (2018) 635.

[22] V. S. Rai, D. Prajapati, V. Kumar, M. K. Verma, S. Pandey, T. Das, N. B. Singh, K. D. Mandal, "Low temperature synthesis, dielectric and electrical characteristics of $Bi_{2/3}Cu_{3-x}Ni_xTi_4O_{12}$ (where x= 0.05, 0.1, and 0.2) ceramics for the dielectric and electrical properties," Journal of Materials Science: Materials in Electronics, **33** (2022) 5273–5282.

[23] V. Kumar, A. Kumar, M. K. Verma, S. Singh, S. Pandey, V. S. Rai, D. Prajapati, T. Das, N. B. Singh, K. D. Mandal, "Investigation of dielectric and electrochemical behavior of $CaCu_{3-x}Mn_xTi_4O_{12}$ (x= 0, 1) ceramic synthesized through semi-wet route," Materials Chemistry and Physics, **245** (2020) 122804.

[24] J. Zhao, M. Chen, Q. Tan, "Embedding nanostructure and colossal permittivity of TiO_2-covered CCTO perovskite materials by a hydrothermal route," Journal of Alloys and Compounds, **885** (2021) 160948.

[25] M. Basak, M. L. Rahman, M. F. Ahmed, B. Biswas, N. Sharmin, "The use of X-ray diffraction peak profile analysis to determine the structural parameters of cobalt ferrite nanoparticles using Debye-Scherrer, Williamson-Hall, Halder-Wagner and size-strain plot: different precipitating agent approach," Journal of Alloys and Compounds, **895** (2022) 162694.

[26] M. Ahmadipour, M. J. Abu, M. F. Ab Rahman, M. F. Ain, Z. A. Ahmad, "Assessment of crystallite size and strain of $CaCu_3Ti_4O_{12}$ prepared via conventional solid-state reaction," Micro & Nano Letters **11** (2016) 147-150.

[27] A. S. Priya, D. Geetha, I. B. ShameemBanu, "Structural, Dielectric, and Impedance Analysis of (Dy, Cu) Co-doped $BiFeO_3$," Brazilian Journal of Physics, **51** (2021) 1438-1447.

[28] G. Wang, S. Yan, J. Sun, S. Wang, Q. Deng, "Visible light photocatalytic and magnetic properties of Nd doped $Bi_2Fe_4O_9$ powders," Journal of Materials Science: Materials in Electronics, **28** (2017) 4371–4377.

[29] S. Sharif, G. Murtaza, T. Meydan, P. I. Williams, J. Cuenca, S. H. Hashimdeen, F. Shaheen, R. Ahmad, "Structural, surface morphology, dielectric and magnetic properties of holmium doped $BiFeO_3$ thin films prepared by pulsed laser deposition," Thin Solid Films, **662** (2018) 83–89.

[30] F. Wang, D. Chen, N. Zhang, S. Wang, L. Qin, X. Sun, "Oxygen vacancies induced by zirconium doping in bismuth ferrite nanoparticles for enhanced photocatalytic performance," Journal of colloid and interface science, **508** (2017) 237-247.

[31] S. R. Naik, T. Shripathi, A. V. Salker, "Preparation, characterization and photoluminescent studies of Cr and Nd co-doped Ce: YAG compounds," Journal of Luminescence, **161** (2015) 335-342.

[32] J. Dai, Z. Li, X. Wen, Q. Wang, "Tuning photocatalytic activity and magnetic behavior of $Bi_{0.8}Re_{0.2}FeO_3$ (Re= Nd, Sm) multiferroics," Journal of Materials Science: Materials in Electronics, **33** (2022) 725–738.

[33] Y. Guo, J. Tan, J. Zhao, "Microstructure and electrical properties of nano-scale SnO_2 hydrothermally coated CCTO-based composite ceramics," Ceramics International, **48** (2023) 17795–17801.

[34] J. Boonlakhorn, P. Suksangrat, P. Thongbai, P. Srepusharawoot, "Improving dielectric properties of (Zn^{2+}, Al^{3+}) Co-doped $CaCu_3Ti_4O_{12}$ perovskite ceramics by enhancing the grain boundary response," Ceramics International, **49** (2023) 23099–23109.

[35] G. D. Zhang, J. Q. Dai, X. L. Liang, "Enhanced ferroelectric properties in La-doped $BiFeO_3$ films by the sol-gel method," Journal of Sol-Gel Science and Technology, **105** (2023) 489-499.

[36] S. Jain, J. Shah, N. S. Negi, C. Sharma, R. K. Kotnala, "Significance of interface barrier at electrode of hematite hydroelectric cell for generating ecopower by water splitting," International Journal of Energy Research, **43** (2019) 4743-4755.

[37] D. Szwagierczak, J. Kulawik, A. Skwarek, "Influence of processing on microstructure and electrical characteristics of multilayer varistors," Journal of Advanced Ceramics, **8** (2019) 408-417.

[38] L. Marchin, S. Guillemet-Fritsch, B. Durand, A. A. Levchenko, A. Navrotsky, T. Lebey, "Grain Growth-Controlled Giant Permittivity in Soft Chemistry $CaCu_3Ti_4O_{12}$ Ceramics," Journal of the American Ceramic Society, **91** (2008) 485-489.

[39] L. Sun, Z. Wang, Y. Shi, E. Cao, Y. Zhang, H. Peng, L. Ju, "Sol−gel synthesized pure $CaCu_3Ti_4O_{12}$ with very low dielectric loss and high dielectric constant," Ceramics International, **41** (2015) 13486–13492.

[40] I. Jalafi, A. Bendahhou, K. Chourti, F. Chaou, S. E. Barkany, M. Abou-Salama, "High permittivity and low dielectric loss of the $(Ca_{0.9}Sr_{0.1})_{1-x}La_{2x/3}Cu_3Ti_4O_{12}$ ceramics," Ceramics International, **49** (2022) 10213–10223.

[41] J. Boonlakhorn, P. Thongbai, B. Putasaeng, P. Kidkhunthod, S. Maensiri, P. Chindaprasirt, "Microstructural evolution, non-ohmic properties, and giant dielectric

response in $CaCu_3Ti_{4-x}Ge_xO_{12}$ ceramics," Journal of the American Ceramic Society, **100** (2017) 3478–3487.

[42] L. Singh, I. W. Kim, B. C. Sin, A. Ullah, S. K. Woo, Y. Lee, "Study of dielectric, AC-impedance, modulus properties of $0.5Bi_{0.5}Na_{0.5}TiO_3$-$0.5CaCu_3Ti_4O_{12}$ nano-composite synthesized by a modified solid state method," Materials Science in Semiconductor Processing, **31** (2015) 386-396.

[43] S. Amhil, S. B. Moumen, A. Bourial, L. Essaleh, "Evidence of large hopping polaron conduction process in strontium doped calcium copper titanate ceramics," Physica B: Condensed Matter, **556** (2019) 36-41.

[44] B. Khan, A. Kumar, P. Yadav, G. Singh, U. Kumar, A. Kumar, M. K. Singh, "Structural, dielectric, magnetic and magneto-dielectric properties of $(1–x)BiFeO_3$-$(x)CaTiO_3$ composites," Journal of Materials Science: Materials in Electronics, **32** (2021) 18012–18027.

[45] K. Abdouli, F. Hassini, W. Cherif, P. R. Prezas, M. P. Graça, M. A. Valent, O Messaoudi, S. Elgharbi, A. Dhahri, L. Manai, "Investigation of the structural, electrical, and dielectric properties of $La_{0.5}Sm_{0.2}Sr_{0.3}Mn_{1-x}Cr_xO_3$ for electrical application," RSC Advanced, **12** (2022) 16805–16822.

[46] U. Venkat, P. Seenuvasakumaran, "Synthesis, structural, micro structural, optical, magnetic and dielectric properties of Nd doped multiferroic bismuth iron oxide," Results in Materials, **17** (2023) 100359.

[47] M. H. Wang, B. Zhang, F. Zhou, "Preparation and characterization of silica-coated $CaCu_3Ti_4O_{12}$," Journal of electronic materials, **43** (2014) 2607-2613.

[48] R. Xue, Z. Chen, H. Dai, D. Liu, T. Li, G. Zhao, "Effects of rare earth ionic doping on microstructures and electrical properties of $CaCu_3Ti_4O_{12}$ ceramics," Materials Research Bulletin, **66** (2015) 254-261.

[49] K. D. Mandal, A. K. Rai, D. Kumar, O. Parkash, "Dielectric properties of the $Ca_{1-x}La_xCu_3Ti_{4-x}Co_xO_{12}$ system (x= 0.10, 0.20 and 0.30) synthesized by semi-wet route," Journal of Alloys and Compounds, **478** (2009) 771–776.

[50] D. Wang, A. Khesro, S. Murakami, A. Feteira, Q. Zhao, I. M. Reaney, "Temperature dependent, large electromechanical strain in Nd-doped $BiFeO_3$-$BaTiO_3$ lead-free ceramics," Journal of the European Ceramic Society, **37** (2017) 1857-1860.

[51] G. Du, F. Wei, W. Li, N. Chen, "Co-doping effects of A-site Y^{3+} and B-site Al^{3+} on the microstructures and dielectric properties of $CaCu_3Ti_4O_{12}$ ceramics," Journal of the European Ceramic Society, **37** (2017) 4653–4659.

[52] J. Boonlakhorn, P. Kidkhunthod, B. Putasaeng, P. Thongbai, "Significantly improved non-ohmic and giant dielectric properties of $CaCu_{3-x}Zn_xTi_4O_{12}$ ceramics by enhancing grain boundary response," Ceramics International, **43** (2017) 2705–2711.

[53] J. W. Lee, J. H. Koh, "Grain size effects on the dielectric properties of $CaCu_3Ti_4O_{12}$ ceramics for supercapacitor applications," Ceramics International, **41** (2015) 10442–10447.

[54] M. Chinnathambi, A. Sakthisabarimoorthi, M. Jose, R. Robert, "Impact of neodymium doping on the dielectric and electrical properties of CCTO synthesized by a facile sol–gel technique," Journal of Materials Science: Materials in Electronics, **32** (2021) 9194–9207.

[55] Q. Zheng, H. Fan, C. Long, "Microstructures and electrical responses of pure and chromium-doped $CaCu_3Ti_4O_{12}$ ceramics," Journal of Alloys and Compounds, **511** (2012) 90–94.

[56] M. F. Ab Rahman, S. D. Hutagalung, Z. A. Ahmad, M. F. Ain, J. J. Mohamed, "Characterization of microstructures evolution on electrical responses of $CaCu_3Ti_4O_{12}$ ceramics," Journal of King Saud University-Engineering Sciences, **28** (2016) 240–245.

[57] J. Mohammed, R. Bhargava, S. Khan, S. Mishra, S. K. Godara, A. K. Srivastava, "Crystal structure refinement, optical properties, dielectric response, and impedance spectroscopy of Ni^{2+}-Co^{2+} substituted bismuth copper titanate (BCTO)," Materials Chemistry and Physics, **248** (2020) 122933.